Journal of Power Sources 195 (2010) 4600–4605

Contents lists available at ScienceDirect

Journal of Power Sources

journal homepage: www.elsevier.com/locate/jpowsour

Highly durable graphene nanoplatelets supported Pt nanocatalysts for oxygen reduction

Yuyan Shao[a], Sheng Zhang[a], Chongmin Wang[a], Zimin Nie[a], Jun Liu[a], Yong Wang[a,b,*], Yuehe Lin[a,*]

[a] Pacific Northwest National Laboratory, Richland, WA 99352, USA
[b] The Gene and Linda Voiland School of Chemical Engineering and Bioengineering, Washington State University, Pullman, WA 99164, USA

ARTICLE INFO

Article history:
Received 29 January 2010
Received in revised form 14 February 2010
Accepted 15 February 2010
Available online 20 February 2010

Keywords:
Graphene nanoplatelets
Polymer electrolyte membrane fuel cell
Oxygen reduction
Durability
Carbon nanotubes

ABSTRACT

We report graphene nanoplatelets (GNPs), which exhibit the advantages of both single-layer graphene and highly graphitic carbon, as a durable alternative support material for Pt nanoparticles for oxygen reduction in fuel cells. Pt nanoparticles are deposited on poly(diallyldimethylammonium chloride) (PDDA)-coated GNP, and characterized with transmission electron microscopy, X-ray diffraction, Raman spectra, and electrochemical tests. Pt/GNP exhibits greatly enhanced electrochemical durability (2–3 times that of Pt/CNT and commercial Etek Pt/C). These are attributed to the intrinsic high graphitization degree of GNP and the enhanced Pt-carbon interaction in Pt/GNP. If considering that GNP can be easily mass produced from graphite, GNP is a promising, low-cost, and durable electrocatalyst support for oxygen reduction in fuel cells.

1. Introduction

Polymer electrolyte membrane (PEM) fuel cell is a high-efficiency and environmentally friendly power source. One of the main obstacles to the commercialization of PEM fuel cells is the high cost and the poor durability of electrocatalytic materials [1,2]. Currently, the most promising electrocatalysts are still carbon supported platinum (Pt/C) [3,4]. Carbon can be electrochemically oxidized under PEM fuel cell conditions, which leads to Pt nanoparticle sintering on or detaching from the support materials and degrades fuel cell performance [1,2,5]. Therefore, much effort has been devoted to develop durable catalyst support materials [6], for example, (graphitized) carbon nanotubes (CNT) [7–10] and graphitic mesoporous carbon (MPC) [11]. But both CNT and MPC have the issue of high cost. Some metal oxides (SnO_2 [12], TiO_2 [13–15], NbO_x [16], etc.) are also developed as catalyst supports or as doping materials of carbon to improve the durability of electrocatalysts. The low conductivity, low specific surface area, and the cost issue are the drawbacks of metal oxides as support materials for fuel cell catalysts [6].

Here, we report a durable electrocatalyst with graphene nanoplatelets (GNPs) as the support, which exhibits 2–3 times durability of commercial Etek Pt/C and Pt/CNT catalysts toward oxygen reduction reaction (ORR).

Graphene has attracted strong scientific and technological interest [17] with great application potentials in various fields, such as electronic devices [18], nanocomposites [19–21], sustainable energy storage and conversion (ultracapacitors [22,23], batteries [24], fuel cells [25–28], and solar cells [29]), bioscience and biotechnologies [30–32]. The graphene nanoplatelets (GNPs) reported here consist of layers (>10) of graphene sheets which might exhibit the advantageous properties of both single-layer graphene (high surface area [33], excellent conductivity [17] and mechanical strength [34], etc.) and highly ordered graphitic carbon (high stability, abundance in source and low cost) [31,35], and avoids the potential weakness of single-/few-layer graphene: poor stability [36], which results from its specific 2D-thin-layer-strcuture. For example, if a single-layer graphene is put in electrochemical corrosive conditions (as in fuel cells [1,2]), both surfaces of graphene sheet are exposed to corrosive reactants (such as reactive oxygen species [O]) which leads to more possibility of carbon atoms being attacked. And it is known that one of the most popular methods for graphene production is chemical/thermal reduction of graphene oxides which is also considered to be the promising strategy for the large-scale production of graphene [37,38]. The chemical/thermal reduction of graphene oxides produces graphene with a lot of chemical and physical defects [38,39]. These chemical/physical defects are expected to make graphene very easy to be oxidized and less stable under harsh electrochemical conditions because the oxidation of carbon materials usually initiates at the defect sites [2,40]. In contrast, GNP that is produced by exfoliating the intercalated graphite [41] retains the highly graphitic structure. Even when

* Corresponding authors. Tel.: +1 509 371 6241; fax: +1 509 376 5106.
E-mail addresses: yongwang@pnl.gov (Y. Wang), yuehe.lin@pnl.gov (Y. Lin).

0378-7753/$ – see front matter © 2010 Elsevier B.V. All rights reserved.
doi:10.1016/j.jpowsour.2010.02.044

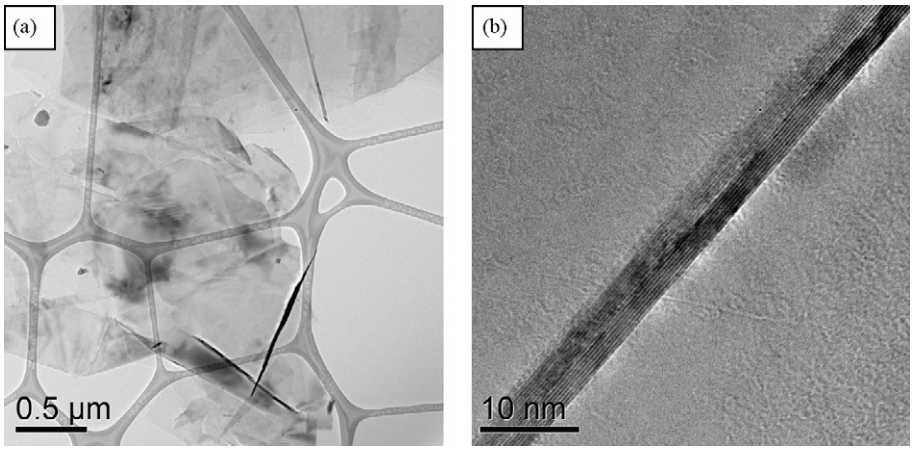

Fig. 1. TEM images of graphene nanoplatelets (GNPs).

the outmost graphene layer is corroded/oxidized, GNP with more graphene layers retains its base graphitic structure. This makes GNP durable under corrosive conditions [42] and is expected to stabilize Pt nanoparticles [31]. If considering that GNP can be directly produced from graphite, GNP is also expected to be much lower in cost than other carbon nanomaterials, such as carbon nanotubes [31,35].

2. Experimental

2.1. Materials, chemicals, and synthesis

Graphene nanoplatelets (XG Sciences, Inc.) were synthesized by exfoliating the sulfuric acid-based intercalated graphite using a microwave oven followed by ultrasonication and milling [20,41]. This usually creates GNP of 5–10 nm in thickness with a specific surface of 100 $m^2\,g^{-1}$. Prior to the deposition of Pt nanoparticles on GNP, GNP was first coated with a long-chain positively charged polyelectrolyte, poly(diallyldimethylammonium chloride) (PDDA) (MW = 200k–350k, Sigma–Aldrich). PDDA can be irreversibly adsorbed onto the hydrophobic surface of GNP via the π–π interaction between the unsaturated C=C contaminant in PDDA chains [43] and graphene plane of GNP. Typically, 300 mg GNPs were dispersed in 500 mL 0.5 wt% PDDA aqueous solution and ultrasonicated for 3 h which yielded a stable dispersion of GNP. Then the dispersed solution of GNP was kept for 24 h under rapid mechanical stirring. After that, 2.5 g KNO_3 was added to increase the attractive action between PDDA and GNP surface and lead to a highly functionalized GNP with PDDA. After stirring for another 24 h, the solution was filtrated and washed with ultrapure DI water (18.2 MΩ cm, Mill-Q Corp.) to remove the free polyelectrolyte and then dried for 3 h at 90 °C in vacuum.

Pt/GNP electrocatalyst was prepared with ethylene glycol (EG) reduction method [11,44]. Typically, 2.656 mL hexachloroplatinic acid (H_2PtCl_6) EG solution (7.53 mg Pt mL^{-1} EG) was added drop by drop into 50 mL EG solution with mechanical stirring for 10 min. 1.0 M NaOH (in EG) was added to adjust the pH of the solution to >13. 80 mg PDDA-functionalized GNP was added to the above solution and stirred for 60 min. The solution was heated in refluxing conditions at 130 °C for 4 h to completely reduce H_2PtCl_6. After cooling down and stirring for 12 h, the pH of the reaction solution was adjusted to <2 with nitric acid solution, which promotes the adsorption of the suspended metal nanoparticles onto the carbon support, then 20 mL ultrapure DI water was added and stirred for 48 h. The resulting catalyst was washed with warm ultrapure DI water until Cl^- was not detected and then dried at 90 °C in vacuum for 3 h. The 20 wt% Pt/GNP electrocatalyst was obtained. Multi-wall carbon nanotubes (Nanolab, USA, used as received) supported Pt/CNT (20 wt% Pt) electrocatalyst were prepared with the same method.

2.2. Materials characterization

The transmission electron microscope (TEM) images of the catalysts were taken in a JEOL TEM 2010 microscope equipped with an Oxford ISIS system. X-ray diffraction (XRD) patterns in θ–2θ scan mode were obtained using a Philips Xpert X-ray diffractometer using Cu Kα radiation at λ = 1.541 Å. Raman spectra were acquired using a Renishaw inVia Microscope using a 514.5 nm Argon laser at 50% power with a 50× aperture.

2.3. Electrochemical measurements

The electrochemical tests were carried out with a CHI660C station (CH Instruments, Inc., USA). Pt wire and Hg/Hg_2SO_4 (scaled to reversible hydrogen electrode [RHE]) were used as the counter electrode and reference electrode, respectively. The working electrodes were prepared by applying catalyst ink onto the pre-polished glass carbon disk electrodes [45]. In brief, 12 mg catalyst was dispersed in 6 mL ethanol, and ultrasonicated to form a uniform black ink. The working electrodes (WE) were prepared by applying 7.5 μL of the well-dispersed catalyst ink onto polished glassy-carbon disk (5 mm in diameter). After dried at room temperature, 10 μL 0.05 wt% Nafion was dropped on the top the catalyst layer to form a thin film protecting catalyst particles from detaching glass carbon disk electrode. Before test, WEs were dried overnight at room temperature.

For electrochemical tests, WEs were first activated with cyclic voltammograms (50 mV s^{-1}, 0–1.1 V) in N_2-purged 0.5 M H_2SO_4 solution until a steady CV was obtained. The linear sweep voltammograms (LSVs) for oxygen reduction reaction (ORR) is measured with a Pine rotating disk electrode test system (Pine Instruments Company, USA) in O_2-saturated 0.5 M H_2SO_4 solution (10 mV s^{-1}, 1600 rpm). The durability tests were carried out in N_2-saturated 0.5 M H_2SO_4 solution with potential step method (1.4 V_10 s to 0.85 V_5 s) for 44 h [45]. This is an in-house developed accelerated degradation tests (ADT) and has been shown to effectively study the catalyst durability with the emphasis on support corrosion [45]. All the tests were conducted at room temperature.

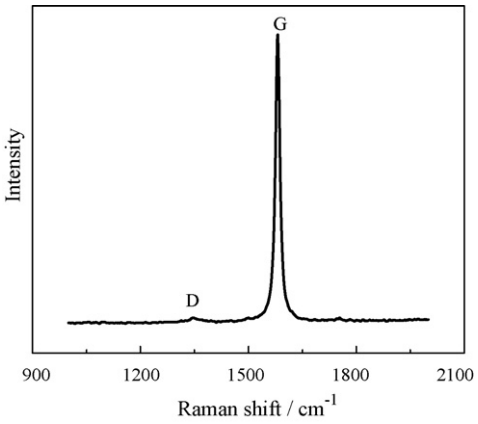

Fig. 2. Raman spectrum of GNP.

3. Results and discussion

Fig. 1 shows typical TEM images of graphene nanoplatelets. GNP exhibits flake structures with various in-plane sizes in the low-resolution image (Fig. 1a). In the high-resolution (HR) TEM image (Fig. 1b), the well-ordered graphene layers can be clearly observed, indicating the high graphitization degree of GNP. The thickness of GNP is <10 nm (~20 graphene layers).

The Raman spectrum of GNP is shown in Fig. 2, which is similar to that of single crystal graphite [46,47]. The narrow and sharp peak at 1580 cm^{-1} corresponds to the G band which is referred to as the "ordered" graphitic band. The peak at 1340 cm^{-1} is referred to as the "disordered" band (D band) [47]. It can be deduced that GNP exhibits an almost perfect ordered graphitic structure since the D band is greatly suppressed in the Raman spectra [42,47], which means that much less structure defects exist on GNP.

Fig. 3 shows the XRD patterns of Pt/GNP, Pt/CNT, and Etek Pt/C, which reveal the diffraction peaks of both carbon and platinum. It can be seen that Pt on the three samples exhibits similar crystalline structures. A sharper and narrower carbon C(0 0 2) diffraction peak appears for Pt/GNP, which indicates a highly graphitic ordered structure of GNP. The presence of C(0 0 4) diffraction peak in Pt/GNP is also the indicative of high crystallinity of the carbon structure in GNP [42,48]. The graphitic structure of carbon can be quantitatively characterized by graphitization index which tells the degree of similarity between a carbon material and a perfect single crystal of graphite [49]. The higher graphitization index indicates a more ordered graphitic structure. Graphitization index (G_{XRD}) can be calculated from the XRD patterns with the following equation (1) [10,49].

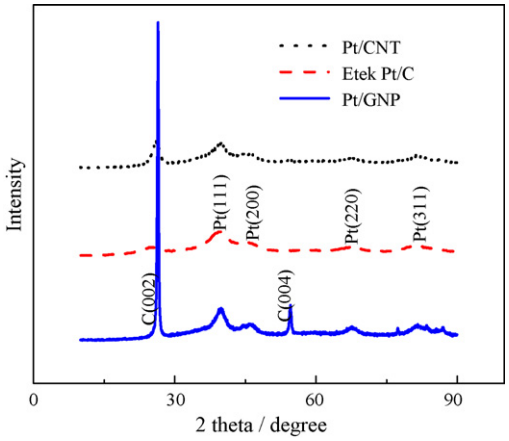

Fig. 3. XRD patterns of Pt/CNT, Etek Pt/C and Pt/GNP.

$$G_{XRD} = \frac{3.440 - d_{0\,0\,2}}{3.440 - 3.354} \quad (1)$$

The results are G_{XRD}(CNT) = 38.4%, G_{XRD}(Etek) = 18.5%, G_{XRD}(GNP) = 87.2% [d_{002}(CNT) = 3.407 Å (2θ = 26.14°), d_{002}(Etek) = 3.424 Å (2θ = 26.01°) and d_{002}(GNP) = 3.365 Å (2θ = 26.47°)]. d_{002} is the interplanar d-space calculated from the ⟨0 0 2⟩ reflection using Bragg's law ($n\lambda = 2d\sin(\theta)$). The highest graphitization index of GNP indicates the highest ordered graphitic structure. This is consistent with the HR-TEM image and Raman spectrum of GNP.

The average stacking height of crystallite in the direction of c axis, Lc, can be calculated from ⟨0 0 2⟩ reflection according to the relation $Lc = 0.89\lambda/B\cos(\theta)$, where λ is the wavelength of the X-rays (1.541 Å), B is the full angular width at half max in radians, and θ is the Bragg angle. Lc of GNP was calculated to be about 8 nm, close to the values from HR-TEM image (Fig. 1b).

Fig. 4 shows the TEM images and Pt nanoparticle distribution of Pt/GNP, Pt/CNT, and commercial Etek Pt/C (Pt nanoparticle distribution of Etek Pt/C was shown in Ref. [45]). Pt nanoparticles are uniformly dispersed on both GNP and CNT. Pt nanoparticles in Pt/GNP exhibit a slightly wider size distribution (Fig. 4d), which might be due to the relatively lower specific surface area of GNP (~100 $m^2\,g^{-1}$ for GNP vs. ~300 $m^2\,g^{-1}$ for CNT). The volume/area averaged diameter ($\bar{d}_{v/a}$), which is considered to well represent the specific surface area of platinum [50], can be calculated from the following equation (2):

$$\bar{d}_{v/a} = \frac{\sum_{i=1}^{n} d_i^3}{\sum_{i}^{n} d_i^1} \quad (2)$$

which are 3.5 nm for Pt/GNP and 3.2 nm for Pt/CNT (3.1 nm for Etek Pt/C [45]). Usually, it is very difficult to deposit metal nanoparticles on such hydrophobic materials as GNP and CNT (if no surface functionalization). PDDA is a long-chain positively charged polyelectrolyte [51], when wrapping hydrophobic carbon, it can effectively trap the negatively charged $[PtCl_6]^{2+}$ (H_2PtCl_6 was used as the precursor of Pt nanoparticles) and stabilize Pt nanoparticles on carbon support, which results in a high dispersion of Pt nanoparticles. The presence of PDDA does not negatively influence the electrochemical performance of Pt nanoparticles [52]. This PDDA-wrapping strategy provides a facile approach for the synthesis of Pt nanoparticles on hydrophobic substrates (avoiding the environmentally unfriendly chemical functionalization process, for example, using strongly oxidizing acid [10,53]), and is widely applicable for the synthesis of metal nanoparticles/hydrophobic substrates composites.

Fig. 5 shows the electrochemical test results of the activity and durability of Pt/GNP, Pt/CNT, and Etek Pt/C toward oxygen reduction. It can be seen that oxygen reduction linear sweep voltammetries (LSVs) (a, c and e) negatively shifted and the hydrogen adsorption/desorption peaks (0–0.4 V) in CVs (b, d and f) were suppressed after the durability test which indicate that ORR overpotentials increase and the electrochemical surface areas (ESA) decrease, respectively, after the durability test. It is obvious that the changes in LSVs (ORR overpotentials) and CVs (hydrogen adsorption/desorption peaks) are much less for Pt/GNP and those for Pt/CNT and Etek Pt/C. All these qualitatively tell that the performance of all the three electrocatalysts degraded after the durability test, and Pt/CNT and Etek Pt/C degraded much more than Pt/GNP. Fig. 5g and h tell the quantitative results. The ESA of Pt were calculated from the hydrogen adsorption/desorption charge in CVs in N_2-saturated 0.5 M H_2SO_4 (210 $\mu C\,cm^{-2}$) [45,54], and oxygen reduction kinetic currents were calculated from the oxygen reduction polarization curves in O_2-saturated 0.5 M H_2SO_4 with the widely used mass-transport correction for rotating disk electrodes

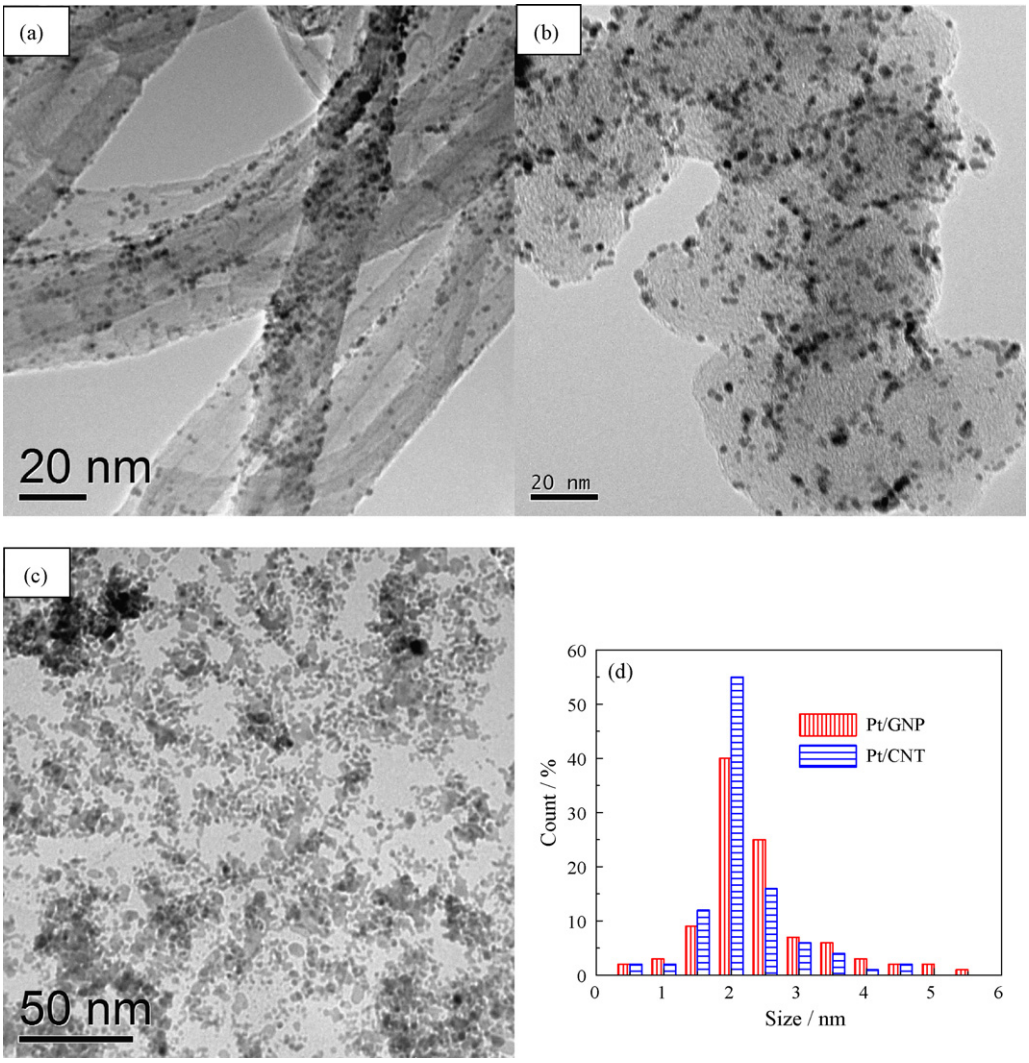

Fig. 4. TEM images of Pt/CNT (a), Etek Pt/C (b) and Pt/GNP (c), and Pt nanoparticle distribution of Pt/CNT and Pt/GNP (d).

[3,55,56]:

$$I_k = \frac{I_d \times I}{I_d - I} \tag{3}$$

where I_k is the mass transfer-free kinetically controlled ORR current, I_d is the measured diffusion-limited current, and I is the experimentally obtained current. It can be seen from Fig. 5g that the activity in terms of the ESA and ORR are comparable for these three samples. Fig. 5h shows the durability of Pt/CNT, Etek Pt/C and Pt/GNP which were characterized with the retaining percentage of the ESA and ORR after the degradation test (44 h). Under the same accelerated degradation test (ADT) condition which has been shown to effectively study the catalyst durability with the emphasis on support corrosion [45], Pt/CNT and Etek Pt/C degraded by ~75% (ESA and ORR), but only ~40% (ESA) and ~20% (ORR) for Pt/GNP, i.e., the degradation rate for Pt/CNT and Etek Pt/C is 2–3 times that of Pt/GNP. Because the Pt nanoparticle sizes and crystallinity are similar for Pt/GNP and Pt/CNT as seen from TEM images and XRD patterns (the only main difference lies in the support materials), it can be concluded that the enhanced durability of Pt/GNP is mainly due to the specific properties of GNP: the intrinsic high graphitization degree. It is known that the electrochemical durability of carbon depends on its graphitic property: more graphitic structure carbon exhibiting higher durability [11,42]. This is because the corrosion of carbon usually starts from the structure defects [2] and carbon with more graphitic phase has much less such defects [57]. This is also confirmed in our pre-experimental study on the electrochemical stability of several kinds of carbon materials: GNP exhibits much higher stability in comparison with (single-/few-layer) graphene, carbon nanotube, and carbon black (GNP exhibits much lower corrosion currents under the same electrochemical condition). As we have analyzed in Introduction, single-/few-layer graphene is easy to be oxidized. It can be deduced that the ratio of carbon atoms on the outmost surface (the exposed carbon atoms) to the total increases with fewer-layer graphene sheets, and in the extreme situation, all carbon atoms in a single-layer graphene are exposed to electrochemical corrosive conditions if, for example, put in a fuel cell which leads to more possibility of carbon atoms being attacked by reactive oxygen species [O]. But for GNP with ~20-layer ordered graphene sheets, the number of outmost carbon atoms is much less. And most graphenes for electrochemical applications are produced from graphene oxides, which intrinsically have a lot of structure defects [38,39]. However, as shown in the above HR-TEM and Raman analysis, GNP exhibits much less defects. In contrast to CNT and carbon black, GNP also exhibits higher graphitization degree. Therefore, GNP is much more stable than any other carbon in this investigation [2,40]. In addition to the high stability of GNP, the enhanced π bonding strength due to the highly graphitic structure in GNP makes Pt-carbon interaction stronger which can also stabilize Pt nanoparticles [2,58].

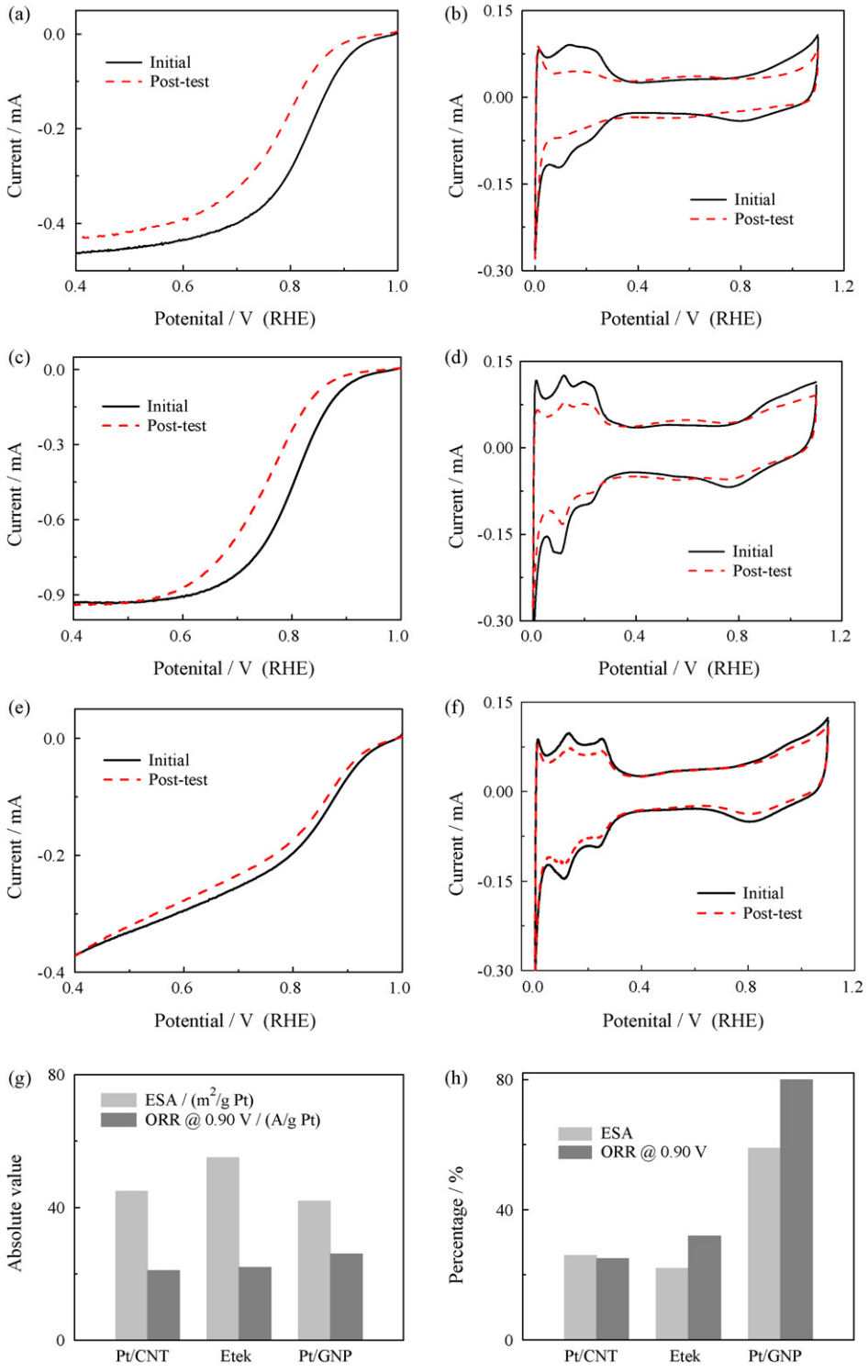

Fig. 5. The oxygen reduction linear sweep voltammetries (LSVs) and the cyclic voltammograms (CVs) on Pt/CNT (a and b), Etek Pt/C (c and d) and Pt/GNP (e and f) electrodes before and after the degradation tests (44 h); (g) the electrochemical surface areas (ESA) and oxygen reduction reaction (ORR) kinetic currents at 0.90 V on fresh Pt/GNP, Pt/CNT, and Etek Pt/C electrodes; (h) the percentage of the retaining ESA and ORR activity on Pt/GNP, Pt/CNT, and Etek Pt/C electrodes after the degradation (44 h). The values of ESA were calculated from the hydrogen adsorption/desorption charge [45,53] in CVs (b, d and f) and ORR kinetic currents were calculated from the LSVs (a, c and e) using the widely used mass-transport correction for rotating disk electrodes [3,54,55]. CVs were recorded in N_2-saturated 0.5 M H_2SO_4 (50 mV s^{-1}, room temperature) and LSVs were recorded in O_2-saturated 0.5 M H_2SO_4 (10 mV s^{-1}, 1600 rpm, room temperature).

4. Conclusion

Graphene nanoplatelets (GNPs), which exhibit the advantages of single-layer graphene and highly graphitic carbon, were employed as an alternative support material for Pt nanoparticles for oxygen reduction. Pt nanoparticles were deposited on PDDA-coated GNP and CNT. The activity of Pt/GNP toward oxygen reduction is comparable to commercial Etek Pt/C and Pt/CNT catalyst. However, the durability of Pt/GNP is greatly enhanced (2–3 times that of Pt/CNT and Etek Pt/C). These are attributed to the intrinsic high graphi-

tization degree of GNP and the enhanced Pt-carbon interaction in Pt/GNP. If considering that GNP can be easily mass produced from graphite, GNP is a promising, low-cost, and durable electrocatalyst support for oxygen reduction in fuel cells.

Acknowledgements

This work is partially supported by the U.S. DOE-EERE HFCIT Program. The characterization was performed using EMSL, a national scientific user facility sponsored by the DOE's Office of Biological and Environmental Research and located at Pacific Northwest National Laboratory (PNNL). PNNL is operated by Battelle for DOE under Contract DE-AC05-76L01830. S. Zhang acknowledges a fellowship from China Scholarship Council and PNNL.

Appendix A. Supplementary data

Supplementary data associated with this article can be found, in the online version, at doi:10.1016/j.jpowsour.2010.02.044.

References

[1] R. Borup, J. Meyers, B. Pivovar, Y.S. Kim, R. Mukundan, N. Garland, D. Myers, M. Wilson, F. Garzon, D. Wood, P. Zelenay, K. More, K. Stroh, T. Zawodzinski, J. Boncella, J.E. McGrath, M. Inaba, K. Miyatake, M. Hori, K. Ota, Z. Ogumi, S. Miyata, A. Nishikata, Z. Siroma, Y. Uchimoto, K. Yasuda, K.I. Kimijima, N. Iwashita, Chem. Rev. 107 (2007) 3904–3951.
[2] Y.Y. Shao, G.P. Yin, Y.Z. Gao, J. Power Sources 171 (2007) 558–566.
[3] H.A. Gasteiger, S.S. Kocha, B. Sompalli, F.T. Wagner, Appl. Catal. B: Environ. 56 (2005) 9–35.
[4] C.J. Zhong, J. Luo, P.N. Njoki, D. Mott, B. Wanjala, R. Loukrakpam, S. Lim, L. Wang, B. Fang, Z.C. Xu, Energy Environ. Sci. 1 (2008) 454–466.
[5] J.F. Wu, X.Z. Yuan, J.J. Martin, H.J. Wang, J.J. Zhang, J. Shen, S.H. Wu, W. Merida, J. Power Sources 184 (2008) 104–119.
[6] Y.Y. Shao, J. Liu, Y. Wang, Y.H. Lin, J. Mater. Chem. 19 (2009) 46–59.
[7] G. Wu, B.Q. Xu, J. Power Sources 174 (2007) 148–158.
[8] Y.Y. Shao, G.P. Yin, Y.Z. Gao, P.F. Shi, J. Electrochem. Soc. 153 (2006) A1093–A1097.
[9] Y.Y. Shao, G.P. Yin, J. Zhang, Y.Z. Gao, Electrochim. Acta 51 (2006) 5853–5857.
[10] J.J. Wang, G.P. Yin, Y.Y. Shao, Z.B. Wang, Y.Z. Gao, J. Phys. Chem. C 112 (2008) 5784–5789.
[11] Y. Shao, S. Zhang, R. Kou, X. Wang, C. Wang, S. Dai, V. Viswanathan, J. Liu, Y. Wang, Y. Lin, J. Power Sources 195 (2010) 1805–1811.
[12] M.S. Saha, R.Y. Li, M. Cai, X.L. Sun, Electrochem, Solid State Lett. 10 (2007) B130–B133.
[13] J. Tian, G.Q. Sun, M. Cai, Q. Mao, Q. Xin, J. Electrochem. Soc. 155 (2008) B187–B193.
[14] S.Y. Huang, P. Ganesan, S.K. Park, B.N. Popov, J. Am. Chem. Soc. 131 (2009) 13898–13899.
[15] H. Chhina, S. Campbell, O. Kesler, J. Electrochem. Soc. 156 (2009) B1232–B1237.
[16] K. Sasaki, L. Zhang, R.R. Adzic, Phys. Chem. Chem. Phys. 10 (2008) 159–167.
[17] A.K. Geim, K.S. Novoselov, Nat. Mater. 6 (2007) 183–191.
[18] J. Hass, W.A. de Heer, E.H. Conrad, J. Phys. Condens. Matter 20 (2008) 27.
[19] T. Ramanathan, A.A. Abdala, S. Stankovich, D.A. Dikin, M. Herrera-Alonso, R.D. Piner, D.H. Adamson, H.C. Schniepp, X. Chen, R.S. Ruoff, S.T. Nguyen, I.A. Aksay, R.K. Prud'homme, L.C. Brinson, Nat. Nanotechnol. 3 (2008) 327–331.
[20] T.R. Hendricks, J. Lu, L.T. Drzal, I. Lee, Adv. Mater. 20 (2008) 2008–2012.
[21] F. He, S. Lau, H.L. Chan, F. Fan, Adv. Mater. 21 (2009) 710–715.
[22] M.D. Stoller, S.J. Park, Y.W. Zhu, J.H. An, R.S. Ruoff, Nano Lett. 8 (2008) 3498–3502.
[23] Y.Y. Shao, J. Wang, M.H. Engelhard, C.M. Wang, Y.H. Lin, J. Mater. Chem. 20 (2009) 743–748.
[24] E. Yoo, J. Kim, E. Hosono, H. Zhou, T. Kudo, I. Honma, Nano Lett. 8 (2008) 2277–2282.
[25] Y.C. Si, E.T. Samulski, Chem. Mater. 20 (2008) 6792–6797.
[26] Y.M. Li, L.H. Tang, J.H. Li, Electrochem. Commun. 11 (2009) 846–849.
[27] R. Kou, Y.Y. Shao, D.H. Wang, M.H. Engelhard, J.H. Kwak, J. Wang, V.V. Viswanathan, C.M. Wang, Y.H. Lin, Y. Wang, I.A. Aksay, J. Liu, Electrochem. Commun. 11 (2009) 954–957.
[28] B. Seger, P.V. Kamat, J. Phys. Chem. C 113 (2009) 7990–7995.
[29] X. Wang, L.J. Zhi, K. Mullen, Nano Lett. 8 (2008) 323–327.
[30] Z. Liu, J.T. Robinson, X.M. Sun, H.J. Dai, J. Am. Chem. Soc. 130 (2008) 10876–10877.
[31] J. Lu, I. Do, L.T. Drzal, R.M. Worden, I. Lee, ACS Nano 2 (2008) 1825–1832.
[32] C.S. Shan, H.F. Yang, J.F. Song, D.X. Han, A. Ivaska, L. Niu, Anal. Chem. 81 (2009) 2378–2382.
[33] M.J. McAllister, J.L. Li, D.H. Adamson, H.C. Schniepp, A.A. Abdala, J. Liu, M. Herrera-Alonso, D.L. Milius, R. Car, R.K. Prud'homme, I.A. Aksay, Chem. Mater. 19 (2007) 4396–4404.
[34] C. Lee, X.D. Wei, J.W. Kysar, J. Hone, Science 321 (2008) 385–388.
[35] M. Segal, Nat. Nanotechnol. 4 (2009) 612–614.
[36] L. Liu, S.M. Ryu, M.R. Tomasik, E. Stolyarova, N. Jung, M.S. Hybertsen, M.L. Steigerwald, L.E. Brus, G.W. Flynn, Nano Lett. 8 (2008) 1965–1970.
[37] C.N.R. Rao, A.K. Sood, K.S. Subrahmanyam, A. Govindaraj, Angew. Chem. Int. Ed. 48 (2009) 7752–7777.
[38] S. Park, R.S. Ruoff, Nat. Nanotechnol. 4 (2009) 217–224.
[39] H.C. Schniepp, J.L. Li, M.J. McAllister, H. Sai, M. Herrera-Alonso, D.H. Adamson, R.K. Prud'homme, R. Car, D.A. Saville, I.A. Aksay, J. Phys. Chem. B 110 (2006) 8535–8539.
[40] A. Barinov, O.B. Malcioglu, S. Fabris, T. Sun, L. Gregoratti, M. Dalmiglio, M. Kiskinova, J. Phys. Chem. C 113 (2009) 9009–9013.
[41] J. Lu, L.T. Drzal, R.M. Worden, I. Lee, Chem. Mater. 19 (2007) 6240–6246.
[42] P.V. Shanahan, L.B. Xu, C.D. Liang, M. Waje, S. Dai, Y.S. Yan, J. Power Sources 185 (2008) 423–427.
[43] D.Q. Yang, J.F. Rochette, E. Sacher, J. Phys. Chem. B 109 (2005) 4481–4484.
[44] W.Z. Li, C.H. Liang, W.J. Zhou, J.S. Qiu, Z.H. Zhou, G.Q. Sun, Q. Xin, J. Phys. Chem. B 107 (2003) 6292–6299.
[45] Y.Y. Shao, R. Kou, J. Wang, V.V. Viswanathan, J.H. Kwak, J. Liu, Y. Wang, Y.H. Lin, J. Power Sources 185 (2008) 280–286.
[46] A.C. Ferrari, Solid State Commun. 143 (2007) 47–57.
[47] F. Tuinstra, J.L. Koenig, J. Chem. Phys. 53 (1970) 1126–1130.
[48] T.W. Kim, I.S. Park, R. Ryoo, Angew. Chem. Int. Ed. 42 (2003) 4375–4379.
[49] C.D. Liang, S. Dai, G. Guiochon, Anal. Chem. 75 (2003) 4904–4912.
[50] P.J. Ferreira, G.J. la O', Y. Shao-Horn, D. Morgan, R. Makharia, S. Kocha, H.A. Gasteiger, J. Electrochem. Soc. 152 (2005) A2256–A2271.
[51] S.P. Jiang, Z.C. Liu, H.L. Tang, M. Pan, Electrochim. Acta 51 (2006) 5721–5730.
[52] S. Zhang, Y.Y. Shao, G.P. Yin, Y.H. Lin, J. Mater. Chem. 19 (2009) 7995–8001.
[53] Y.C. Xing, J. Phys. Chem. B 108 (2004) 19255–19259.
[54] Y.Y. Shao, G.P. Yin, J.J. Wang, Y.Z. Gao, P.F. Shi, J. Electrochem. Soc. 153 (2006) A1261–A1265.
[55] J. Zhang, K. Sasaki, E. Sutter, R.R. Adzic, Science 315 (2007) 220–222.
[56] B. Lim, M.J. Jiang, P.H.C. Camargo, E.C. Cho, J. Tao, X.M. Lu, Y.M. Zhu, Y.A. Xia, Science 324 (2009) 1302–1305.
[57] D. Bom, R. Andrews, D. Jacques, J. Anthony, B.L. Chen, M.S. Meier, J.P. Selegue, Nano Lett. 2 (2002) 615–619.
[58] G. Gupta, D.A. Slanac, P. Kumar, J.D. Wiggins-Camacho, X.Q. Wang, S. Swinnea, K.L. More, S. Dai, K.J. Stevenson, K.P. Johnston, Chem. Mater. 21 (2009) 4515–4526.